Peer Reviewed Paper openaccess

Characterisation of oxide layers on technical copper based on visible hyperspectral imaging

Jan Stiedl,[a] Georgette Azemtsop M.,[b] Barbara Boldrini,[c] Simon Green,[d] Thomas Chassé[e] and Karsten Rebner[f,*]

[a]University of Tuebingen, Institute of Physical and Theoretical Chemistry, Auf der Morgenstelle 18, 72076 Tuebingen, Germany; Reutlingen University, Process Analysis & Technology, Alteburgstrasse 150, 72762 Reutlingen, Germany; Robert Bosch GmbH, Automotive Electronics, Postfach 1342, 72703 Reutlingen, Germany. https://orcid.org/0000-0001-5553-8631

[b]Reutlingen University, Process Analysis & Technology, Alteburgstrasse 150, 72762 Reutlingen, Germany. https://orcid.org/0000-0001-9558-6603

[c]Reutlingen University, Process Analysis & Technology, Alteburgstrasse 150, 72762 Reutlingen, Germany. https://orcid.org/0000-0003-1357-8453

[d]Robert Bosch GmbH, Automotive Electronics, Postfach 1342, 72703 Reutlingen, Germany

[e]Center for Light-Matter Interaction, Sensors & Analytics (LISA$^+$), Auf der Morgenstelle 15, 72076 Tuebingen, Germany. https://orcid.org/0000-0001-6442-8944

[f]Reutlingen University, Process Analysis & Technology, Alteburgstrasse 150, 72762 Reutlingen, Germany.
E-mail: karsten.rebner@reutlingen-university.de, https://orcid.org/0000-0002-3577-2903

The detection and characterisation of oxide layers on metallic copper samples plays an important role for power electronic modules in the automotive industry. However, since precise identification of oxide layers by visual inspection is difficult and time consuming due to inhomogeneous colour distribution, a reliable and efficient method for estimating their thickness is needed. In this study, hyperspectral imaging in the visible wavelength range (425–725 nm) is proposed as an in-line inspection method for analysing oxide layers in real-time during processing of copper components such as printed circuit boards in the automotive industry. For implementation in the production line a partial least square regression (PLSR) model was developed with a calibration set of $n = 12$ with about 13,000 spectra per sample to determine the oxide layer thickness on top of the technical copper surfaces. The model shows a good prediction performance in the range of 0–30 nm compared to Auger electron spectroscopy depth profiles as a reference method. The root mean square error (RMSE) is 1.75 nm for calibration and 2.70 nm for full cross-validation. Applied to an external dataset of four new samples with about 13,000 spectra per sample the model provides an RMSE of 1.84 nm for prediction and demonstrates the robustness of the model during real-time processing. The results of this study prove the ability and usefulness of the proposed method to estimate the thickness of oxide layers on technical copper. Hence, the application of hyperspectral imaging for the industrial process control of electronic devices is very promising.

Keywords: hyperspectral imaging, pushbroom imaging, copper oxide, oxide layer thickness, multivariate analysis, partial least square regression, prediction, reflectance

Correspondence
K. Rebner (karsten.rebner@reutlingen-university.de)

Received: 28 November 2018
Revised: 26 April 2019
Accepted: 26 April 2019
Publication: 18 June 2019
doi: 10.1255/jsi.2019.a10
ISSN: 2040-4565

Citation
J. Stiedl, G. Azemtsop M., B. Boldrini, S. Green, T. Chassé and K. Rebner, "Characterisation of oxide layers on technical copper based on visible hyperspectral imaging", *J. Spectral Imaging* **8,** a10 (2019). https://doi.org/10.1255/jsi.2019.a10

Introduction

An important trend in the current technological development within the electronics industry is miniaturisation, which has led to the creation of new field microelectromechanical systems.[1,2] At present, many devices and objects produced have very small sizes, down to the nanometre level. The progress of microelectromechanical systems technology is essential for a considerable reduction of costs, adverse effects on the environment, and energy and material consumption.[1] Electronic circuit boards represent the main components of power semiconductor modules and their most important constituent material is copper, in particular in the form of copper lead frames.

The surface quality of copper substrates plays an important role in the reliability, quality and lifetime of the final product, i.e., the power electronic module. A clean substrate surface increases the effectiveness of attaching processes, including gluing, wire bonding and moulding;[3] therefore, contaminants such as oxide layers on the substrate surface must be removed before the start of any of these processes.[4] Surface cleanliness of electronic circuit boards extends the product lifetime by ensuring adequate adhesion and good electrical and thermal performance.[5]

The great advantages of copper, including its low bulk electrical resistivity and high resistance to electromigration and stress migration, determine its attractiveness for the electronics industry,[6] and it has long been considered as a promising interconnection material in the fabrication of semiconductor devices. Thus, understanding the mechanism of copper oxidation is crucial to control the thickness, homogeneity and nature of the formed oxide layers.[7] Since copper is susceptible to oxidation when exposed to oxidants such as oxygen or water at elevated temperatures, its degree of oxidation is believed to be affected by environmental conditions, temperature, exposure time and surface impurities;[8] generally, the thickness of the oxide layers increases with the oxidation time and temperature.[9] During the oxidation process, copper is oxidised first to copper (I) oxide (CuO_2), also called cuprous oxide, and then to copper (II) oxide (CuO), known as cupric oxide.[10]

The formation and growth of copper oxide layers during the oxidation of metallic copper may be related to thin film interferences in the refracted visible light, resulting from the changes in the refractive index from air to thin oxide film and copper substrate.[11] Copper oxidation can be investigated either by surface science or optical methods. Surface science methods include the use of techniques such as Auger electron spectroscopy (AES), X-ray photoelectron spectroscopy (XPS) and secondary ion mass spectrometry (SIMS).[12,13] Gaining information with these physical methods requires ultrahigh vacuum conditions, which makes difficult their application for the online and in-line characterisation of oxide layers. The optical properties of metal oxides have been extensively studied by several researchers using ultraviolet–visible–near infrared (UV–Vis–NIR) diffuse reflectance spectroscopy, Raman spectroscopy and Fourier transform infrared spectroscopy (FTIR).[14,15] These techniques are more suited for application in manufacturing processes because of their ability to allow a relatively quick, simple and non-destructive analysis of the material; Whiteside *et al*. presented a detailed review of the techniques for the characterisation of metallic thin films.[16]

Diffuse reflectance spectroscopy has been used to estimate the oxide layer thicknesses of various metals including zinc,[17] cobalt[18] and chromium.[19] Sanchez *et al*. performed UV–Vis diffuse reflectance spectroscopy in the 200–700 nm range to study the nature of oxide films formed on copper surfaces and observed that the Vis–NIR absorbance of the copper oxides increased with its layer thickness, since the change in the reflectance is proportional to the thickness.[20] Dahrul *et al*. similarly reported the influence of the film thickness on the properties of the copper oxides; they recorded the VIS–NIR absorbance spectra of three copper oxide layers formed at different temperatures (350 °C, 450 °C and 550 °C), revealing that these layers had the most prominent absorption band in the visible region (at 470 nm) and, furthermore, that the one formed at 550 °C had the highest absorbance intensity, which was explained by the presence of more copper oxide crystals absorbing the photon energy.[21] These results agree with those achieved by Shui *et al*. by using UV–Vis spectroscopy in the 200–800 nm range. The authors investigated the properties of copper oxide layers prepared by sonochemical synthesis and found that their optical properties were strongly affected by their morphology.[10]

According to Lenglet *et al.*, the absorption band of copper oxides in the range of 450–630 nm is mostly due to the copper and oxygen vacancies in the oxide crystal structure caused by the transformation of Cu_2O into

Cu_3O_2 at temperatures below 300 °C,[22] and this assertion agrees with the study of Machefert *et al.*[23]

Despite the several studies focused on the characterisation of copper oxide films, the sample homogeneity remains a big challenge in the estimation of their thicknesses over the complete surface. The possibility to determine the copper oxide layer thickness via UV–Vis diffuse reflectance spectroscopy has been demonstrated in a previous work.[24] However, different contamination sources may lead to an uncontrolled growth of the oxide layer; since an inspection technique such as UV–Vis diffuse reflectance spectroscopy is typically carried out at a specific location on the substrate surface, the oxide film thickness estimation could significantly be affected by the heterogeneity of the substrate surface. Hence, a new procedure should be employed to overcome the problem of surface inhomogeneity of the oxide layer. From this viewpoint, this study focused on the locally resolved detection and quantification of copper oxide layers by means of hyperspectral imaging (HSI).

The following sections illustrate some of the various applications of pushbroom HSI systems in diffuse reflectance; it is worth emphasising that reflectance is the most employed mode of HSI.[25]

The most common industrial branches in which HSI is applied are the food and pharmaceutical industries. HSI is commonly performed in the visible range to determine the freshness of meat,[26,27] tomatoes[28] and fruits[29] in the food industry as well as the product quality and safety[30] in both of them.

Wollmann *et al.*[31] focused on the use of HSI systems to predict the strength of mechanical components bonded on a substrate. Since the presence of thin solid films on a substrate may strongly influence the bonding process, some investigations on these films by HSI have been started.

Gruber *et al.*[32] performed reflectance HSI in the Vis–NIR range (400–1000 nm) to characterise Al_2O_3 layers on stainless steel foils used for battery production. By combining this method with multivariate analysis (MVA), they could predict the thickness of the Al_2O_3 layers using four latent variables. The results of the partial least square regression (PLSR) model showed a RMSE of 2.43, indicating a reliable prediction power for the thin film thickness. The authors tried to extend the study by defining quality control parameters, such as uncoated area percentage and mean layer thickness, for a possible automated in-line application. HSI remains a challenging technique due to the strong variations in the mean layer thickness of the samples. A similar work conducted by Ham *et al.* confirmed the ability of HSI to identify Al_2O_3 and SiO_2 thin films and quantify their thickness; they observed a positive correlation between the oxide layer thickness and the material absorbance.[33]

Wollmann *et al.*[34] demonstrated the capability of HSI to determine the sheet resistance and conductivity of conductive thin films. They studied a transparent conductive oxide (indium tin oxide) film. Since high sheet resistance is characteristic of substrate defects (contaminations or cracks), which can be visualised on the distribution map derived from the HSI images, this technique allows the evaluation of the surface contamination of a substrate; a patent for this work was filed in 2015.

In the current study, we will extend the list of HSI applications in the detection and characterisation of oxide films on metal surfaces. To the best of our knowledge, this is the first work reporting the identification and quantification of copper oxide thin films by HSI.

Materials and methods

Sample preparation

In total, 16 copper sheets were provided by Wieland-Werke AG (Wieland K-14, Cu ≥ 99.95 %, P ≈ 0.003 %, 5.0 × 3.0 × 0.8 cm). They were first ultrasonically cleaned at 50 °C for 5 min with Vigon A 200 (Zestron) as cleaning medium and then rinsed with deionised water for 3 min. The copper sheets were oxidised at two different temperatures (150 °C and 175 °C) for ten different oxidation times. The oxidation temperature and times are used because they are used as standard parameters for transfer moulding.

Oxide layer thickness measurement

The thicknesses of the oxide layers were determined by depth profiling using AES, details were reported elsewhere.[24] Twelve of the sixteen samples were used for the PLSR calibration and the remaining four for validating the PLS model.

Hyperspectral image collection and processing

Vis hyperspectral imaging system

A hyperspectral pushbroom imaging system covering the spectral range of 425–725 nm, with a spectral resolution

of 8 nm, was used to acquire the hyperspectral images of copper samples in the reflectance mode. The system consists of a 12-bit 640 × 480 pixels charged-coupled device camera (PixelFly PCO VGA; PCO AG, Kelheim, Germany) and a spectrograph equipped with an optical slit of 50 µm (ImSpector V8 ½, specim; Spectral Imaging Ltd, Oulu, Finland) and an 8.5-mm lens (1 : 1.5 television lens; Cosmicar, Japan). Additional components included a conveyor belt (Umbio), a computer equipped with the CamWare V3.06 software (PCO imaging, Kelheim, Germany) for data acquisition, and a 50-W tungsten halogen light source (Radium Lampenwerk GmbH, Germany) oriented at 45 ° with respect to the horizontal plane.

The Red–Green–Blue (RGB) images were acquired using a Canon PowerShot G12 digital camera, with the following parameters: shutter speed: 1/60 s, ISO-320, f/3.5. For multivariate analysis of the images, they were converted to single-wavelength-based RGB images (red: 650 nm, green: 500 nm, blue: 450 nm).

Image acquisition and calibration

The hyperspectral images were recorded in reflectance mode using a camera exposure time of 12 ms. The conveyor belt speed was set to 2.75 mm s^{-1} and the distance between the optical instrument and the sample was about 26 cm. The raw images acquired by the HSI system were corrected with white reference image I_{white} and dark image I_{dark}[35] into reflectance units.

Image processing and MVA

The whole data analysis and image processing were performed using the Evince Prediktera 2.7.9 software (UmBio AB, Umeå, Sweden). To remove the background of the samples and bad pixels, a principal component analysis (PCA) with two components, explaining 97.02 %, was used.

In this study, a PLSR calibration model was built for a data set of 12 samples ($n = 12$) and validated with the leave-one-out cross-validation technique, used as full cross-validation method.[36] An external validation was further performed to evaluate the performance of the developed calibration model on the samples of the prediction set. The partitioning of the samples into calibration and validation set as well as the corresponding oxide layer thickness are shown in Table 1. Unfortunately, there was a detector error while measuring two samples (2 min and 8 min at 175 °C) which led to some pixel failures; these were excluded for analysis.

In order to decrease the effects of random noise, spectral preprocessing algorithms such as Savitzky–Golay smoothing with 23 points and baseline correction were used. These algorithms reduce unessential effects on the data extracted from the hyperspectral images and, thus, improve the robustness and predictive ability of the model.

The performances of the calibration and prediction models were evaluated based on the coefficients of determination (R^2) and the RMSEs, respectively designated as R^2_C and RMSEC for the calibrating process, R^2_V

Table 1. Determined thicknesses for oxide layers, formed with different oxidation times at 150 °C and 175 °C, using the PLS model.[24]

Oxidation time (min)	Oxidation temperature: 150 °C Oxide layer thickness (nm)	Oxidation temperature: 175 °C Oxide layer thickness (nm)	Used for
0	1.8	1.8	Calibration
1	3.5	3.1	Calibration
2	5.4	5.4	Validation
3	7.4	7.9	Calibration
4	9.4	10.6	Validation
5	11.5	13.3	Calibration
6	13.5	16.1	Validation
7	15.5	18.8	Calibration
8	17.5	21.6	Validation
10	21.4	27.1	Calibration

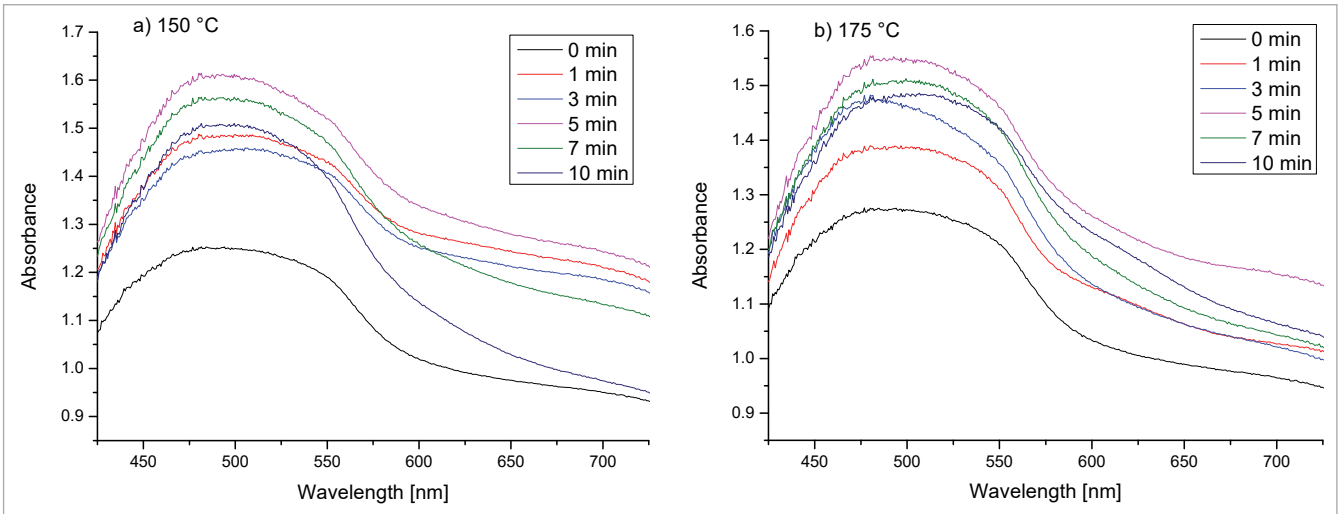

Figure 1. Reflectance spectra obtained by averaging 13,000 spectra in the wavelength range from 425 nm to 725 nm of copper substrates oxidised at a) 150 °C and b) 175 °C. The oxidation time of each sample is given in minutes.

and RMSECV for the cross-validation process, and R_P^2 and RMSEP for the prediction process. Generally, an optimal model should provide high values of R_C^2, R_V^2 and R_P^2 and low values of RMSEC, RMSECV and RMSEP;[36,37] however, the prediction accuracy of a model is evaluated based on the (small) difference between RMSEC and RMSEP.[38]

Results and discussion

Spectral features of copper oxides

Figure 1 shows the absorption spectra averaged over all the 12 samples for the calibration set, calculated for the various oxidation times and temperatures. A copper substrate spectrum is composed of overlapped spectra of metallic copper and copper oxides. Therefore, the spectral signatures of the samples contain useful information correlated with the score images Figure 2); in other words, at a specific wavelength, a sample with low absorbance (high reflectance) has a high proportion of blue in the score image, while one with high absorbance (low reflectance) shows a higher proportion of red.

The difference observed in the absorbance could be attributed to the different oxide layer thicknesses of each sample. Copper is known as a shiny material with high reflectance in the visible wavelength range and absorbance of the red light. However, the formation of oxide layers on its surface increases the refractive index and reduces the extinction coefficient, diminishing the reflectance and thus increasing the absorption capability of the material. Hence, the broad band in the range from 406 nm to around 550 nm is associated with the strong absorption of Cu_2O and, as the wavelength increases, the refractive index and the extinction coefficient decrease, enhancing the absorption in this spectral region.[39]

The comparison between the averaged spectra obtained by the HSI system and classical spectroscopy from the previous work[24] revealed some differences in the wavelength range around 450 nm, which was due to the limited spectral range of the pushbroom imager working at the lower limit at this point. In addition, the set-up was different due to the use of an integrating sphere.

Figure 1 shows the effect of oxidation time and temperature on the spectra of the copper samples with an increase of the absorbance. The oxidation time increased considerably the absorbance of the copper substrates in the range of about 406–550 nm, while only a slight increase was observed when varying the oxidation temperature. Thus, the absorbance of copper increases with the oxidation time and temperature (Figure 1), as reported in the literature.[39]

Figure 2 shows the score and the classical RGB images of each sample of the calibration set. Apparently, no visible symptoms of oxidation stress can be observed in the RGB images. Since the PLSR model based on the RGB images was not satisfactory, the one based on the

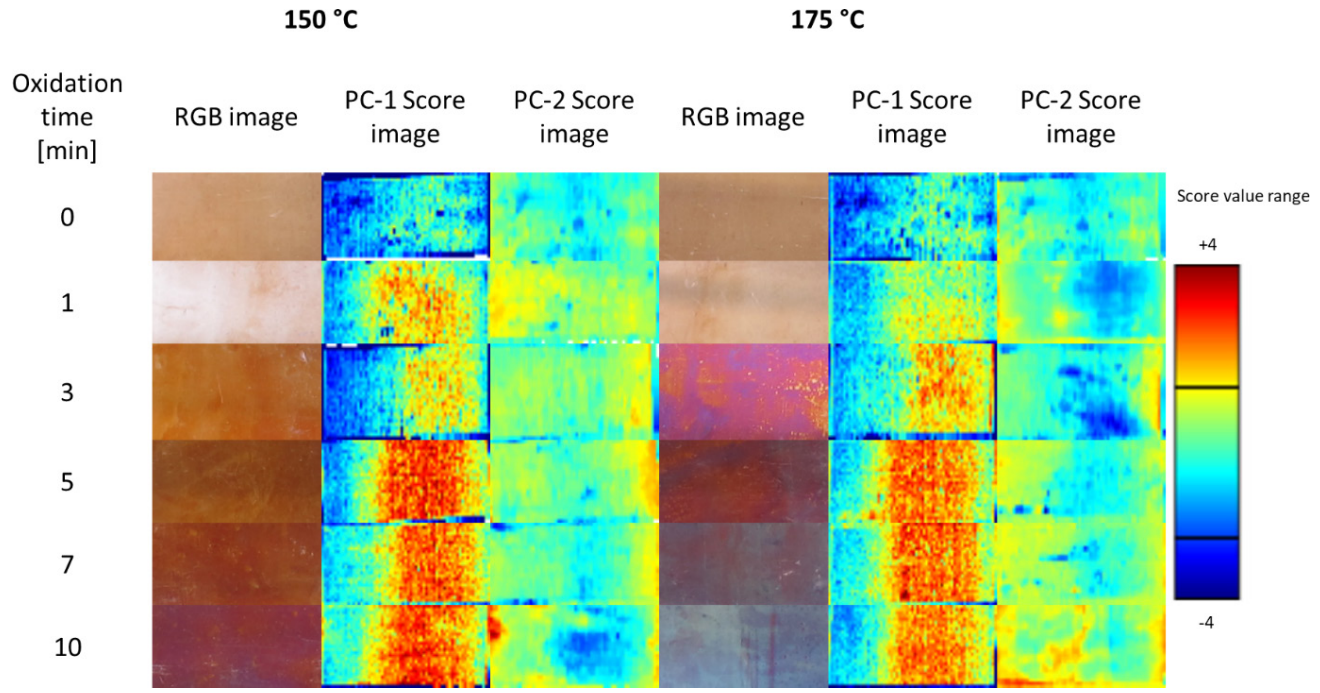

Figure 2. Score and RGB images of copper substrates obtained from the calibration set, oxidised at different times and temperatures. The coloured pixels represent the oxide content, from low (blue) to high (red). The black squares show the area for calculation of the average spectra for each sample (PC1 92.9 %, PC2 4.12 %).

Vis spectra was built up. Clear differences between the samples were observed according to the oxidation time and temperature.

Development of a calibration model

The PLSR model for estimating the oxide layer thickness was established using the mean spectra of each of the 12 copper substrates from the highlighted areas shown in Figure 2, which were considered as the **X**-matrix, while the **Y**-matrix was designed from the oxide layer thickness values obtained by using the approach described in the previous work using AES depth profiling.[24] The optimal number of latent variables (LV) is determined by the lowest RMSECV and highest R^2.[40] In this study, the optimal PLSR model was obtained using four LVs. Figure 3 shows the correlation between the reference values and those calculated from the HSI spectral information, and a linear fit can be observed between the two sets of values.

In Figure 3, the sample points are very close to the linear fit, indicating a very good model fitting. The calibration and cross-validation processes provided, respectively, $R^2_C = 0.99$ with RMSEC = 1.75 nm and $R^2_{CV} = 0.90$ with RMSECV = 2.70 nm, implying a good performance of the model. By using four LVs, the variance explained by the model for the X- and Y-variables was 98 % and 90 %, respectively, indicating that four PLS components are sufficient to describe most of the variance in the data according to the spectral information. The R^2_{CV} value of 0.90 proves the good predictive power of the applied model. In addition, the relative error of the calibration model, calculated by means of the highest predicted oxide layer thickness value (30.3 nm) and the RMSECV, was about 8 %, and such a small percentage of deviation further confirms the good performance of the model. According to the cross-validation results, it can be stated that the PLSR model was suitable for estimating the thickness of the copper oxide layers. The first four PLS weights of the regression model, which describe the copper oxide content in the spectral range of 425–725 nm, are shown in Figure 4 as follows: the fourth vector has the highest number of sensitive wavelength ranges and, similarly to the mean absorbance spectra (Figure 1), describes the main information at approximately 508 nm because the regression coefficient in the PLS model is the highest at this wavelength. This indicates that four LVs are sufficient for a reliable extraction of the relevant information for estimating the thickness of copper oxide layers.

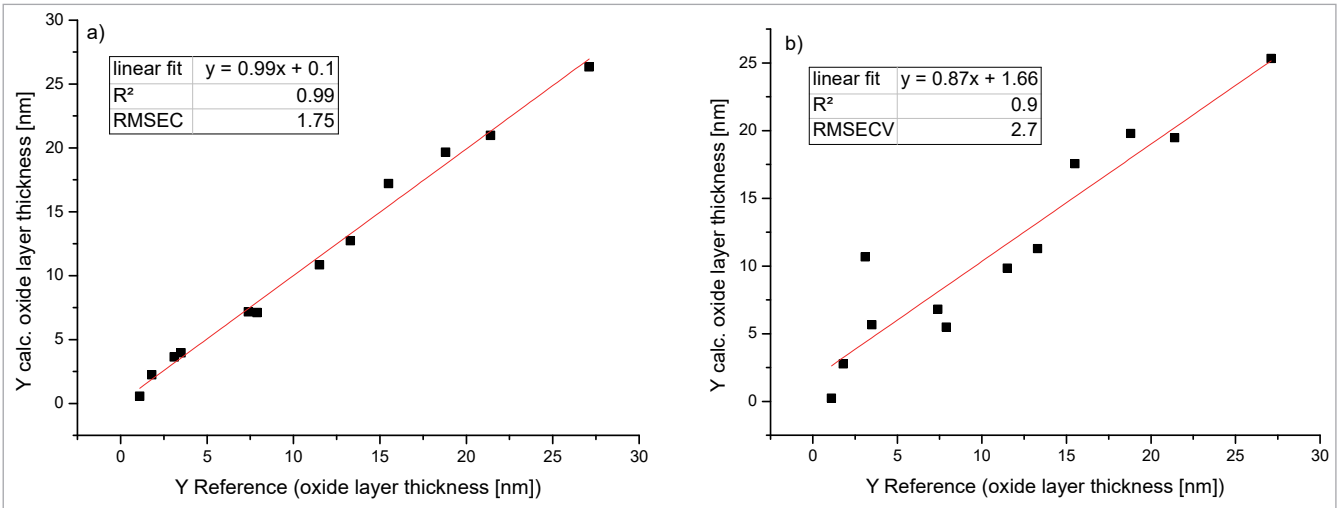

Figure 3. Partial least square regression (PLSR) plots between reference and measured oxide layer thicknesses for the visible spectra obtained from a) the calibration set ($n = 12$) using four PLSR components and b) the results of the full cross-validation. RMSEC and RMSECV are the root mean square errors of the calibration and cross-validation processes, respectively, and also the determination coefficients (R^2) are shown.

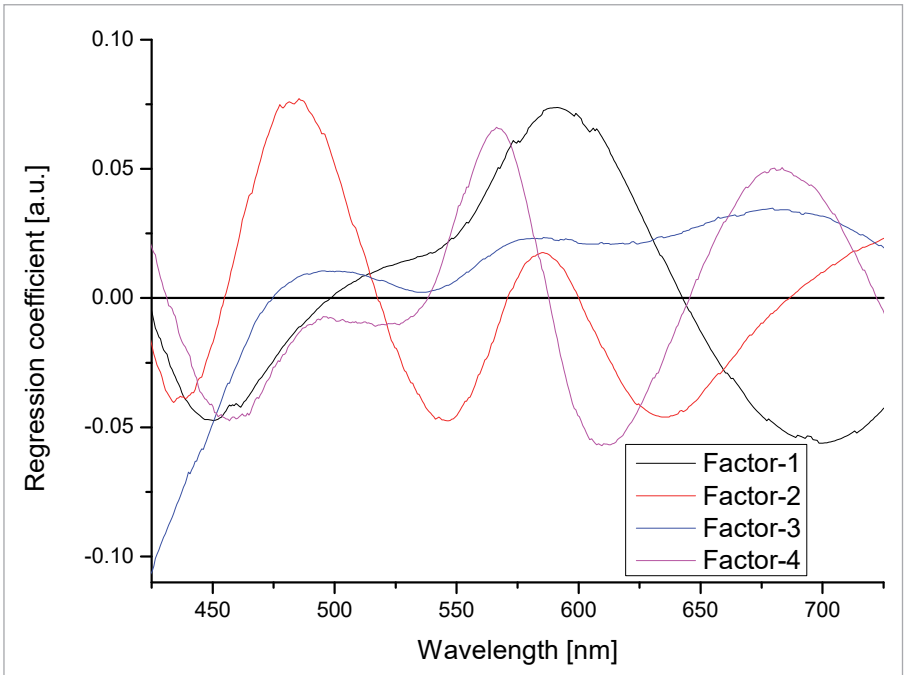

Figure 4. Regression coefficient plot obtained from the PLS model built on the calibration set for the prediction of the copper oxide layer thickness.

Prediction based on PLSR

To assess the predictive ability of the PLSR model built on the calibration set, a prediction set containing four samples oxidised at 175 °C for 2, 4, 6 and 8 min was used for an external validation. The results indicated that the PLSR model was very effective in predicting the oxide layer thickness, with $R^2_{CV} = 0.90$ and RMSECV = 2.70 nm. Using this model for predicting the same attribute for the samples of the validation set achieved a powerful predictive ability, with $R^2_P = 0.95$ and RMSEP = 1.84 nm. Figure 5 shows the correlation between the reference values and those predicted based on the PLSR. To achieve a better statement of the complete surface, we divided the surface into five equal-sized areas. The linear fit indicates

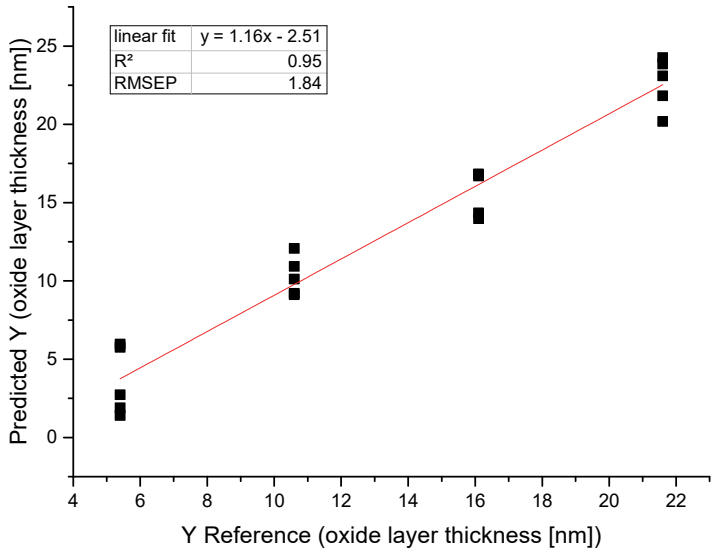

Figure 5. Reference vs predicted copper oxide layer thicknesses plot based on the external validation set.

that the testing values are almost equal to the reference ones. The closer the sample point to the diagonal line, the better the model. The small error rates and high square correlation coefficients confirm that the model attained accurate predictions.

To get a more visual impression of the inhomogeneity of the oxide layer thickness, the thickness for every pixel from the prediction and calibration sets was predicted and plotted in Figure 6. The difference in the layer thickness within one sample increases with oxidation time. This is due to some areas on the surface where the oxidation is not too strong.

The interpretation of the predicted false-colour images of all sets shown in Figure 6 indicates an inhomogeneous thickness of the oxide layers. The thicker the oxide layer, the less inhomogeneous the visual impression. For more tangible data, the high variance can be explained with R_C^2, R_{CV}^2, R_P^2, RMSEC, RMSECV and RMSEP. The high regression coefficients and low absolute errors prove the robustness of the calibration and prediction models. The prediction accuracy of a model is evaluated based on the difference between RMSEC and RMSEP: the smaller this difference, the more accurate the model.[41] In this study, the absolute difference between RMSEC and RMSEP was small (0.09 nm), demonstrating the robustness and accuracy of the developed models. The obtained results prove the ability and reliability of hyperspectral push-broom imaging systems for estimating the thickness of copper oxide layers on metallic copper substrates. All in all, the results show that the application can be used to determine the oxide layer thickness on technical copper surfaces. Before installing the measurement equipment at the production line, there should be a more detailed experiment plan with real samples. Due to the measurement set-up, the roughness of the surface directly influences the reflectance of light on the surface. By having real samples with a very large inhomogeneous roughness, the power of the model could be affected. In order to avoid deterioration of the predictive power of the model, a new sample set is needed. The given sample set in this study was chosen because of the wide range of oxide layer thicknesses. If a smaller range of thicknesses is representative of production samples, the model should be adapted to this particular range. For example, there are some sources in the literature, which found a critical oxide layer thickness for adhesion of mould compounds that could be set as a scope for production.[42–46] By implementing the HSI system to a production line, this parameter could be tracked for all parts. In the end the use of a HSI system leads to an extreme reduction of time. Each measurement of an oxidised sample with the AES depth profiling system needs approximately four hours of work. In contrast to that, a HSI measurement needs around a few seconds.

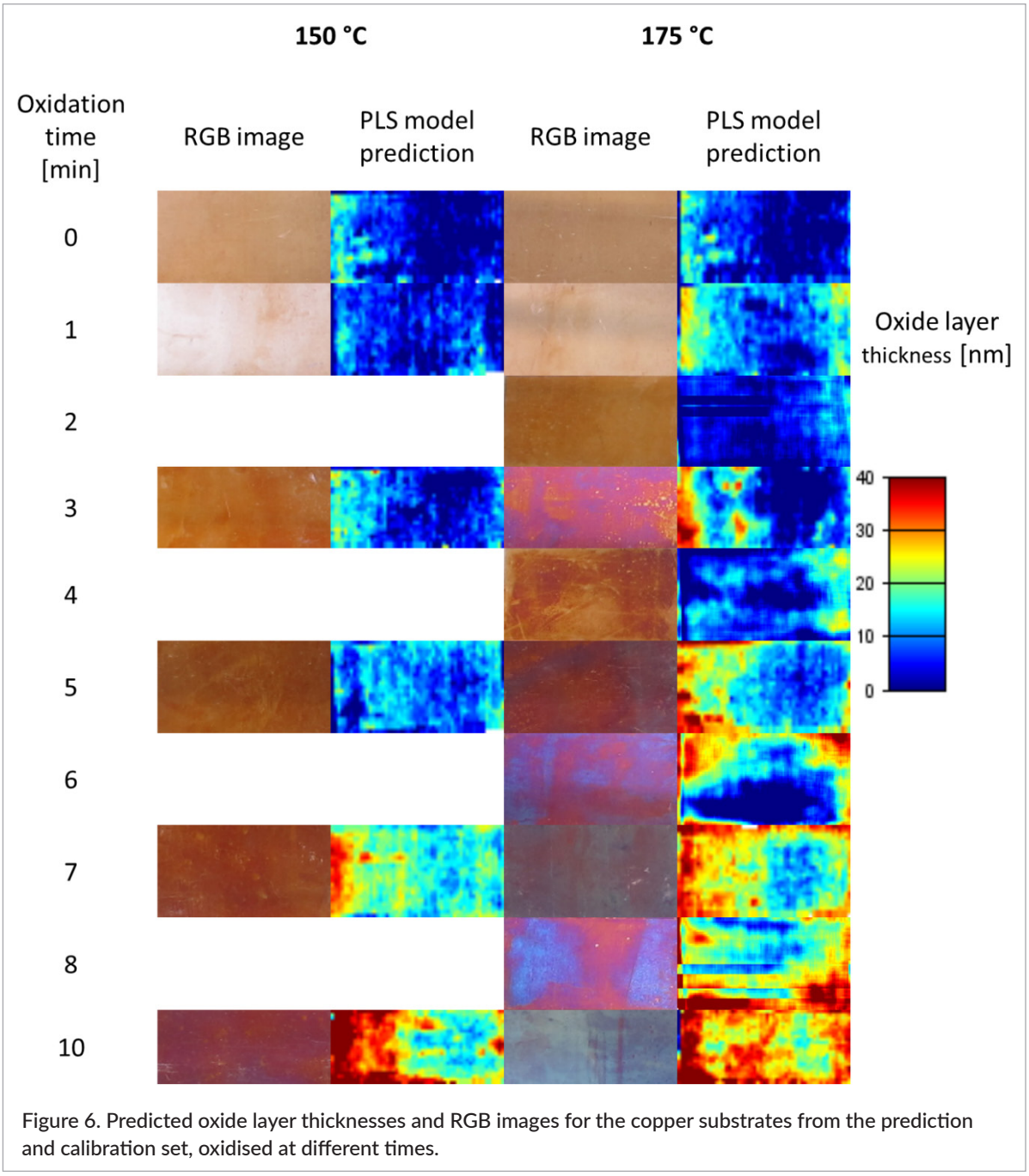

Figure 6. Predicted oxide layer thicknesses and RGB images for the copper substrates from the prediction and calibration set, oxidised at different times.

Conclusions

Copper substrates are used in the fabrication of numerous electronic devices due to the great advantages offered compared to other metals. The chemical composition and physical structure of copper substrates influence the process control and the characteristics of the final electronic products. The aim of this study was to demonstrate the capability of the HSI technique in monitoring copper-based materials and provide spectral information about their chemical composition. In particular, this study reports for the first time the use of HSI to predict the thickness of the copper oxide layers formed on metallic copper materials.

The results demonstrated that HSI combined with PLSR provides a tool for rapid and non-destructive oxide film analysis, which accurately predicted the oxide layer thickness of test copper sheets. In the visible range (425–725 nm), the PLSR model with four PLS components

provided, for the cross-validation process, a determination coefficient of 0.90 and a RMSE of 2.70 nm. The external prediction based on the PLSR model also exhibited a good performance, with a determination of 0.95 and a RMSE of 1.84 nm.

The performance of this technique in terms of prediction accuracy was compared to that of conventional spectroscopy. The low absolute difference (0.86 nm) observed between the validation and prediction errors confirmed the robustness and good quality prediction of the proposed HSI technique, although a better prediction of quality attributes would require a larger sample size.

The rapid and accurate measurement of copper oxide layer thickness is important for reducing the waste rate and manufacturing costs of electronic devices and consequently increasing the final product quality. In this viewpoint, the use of pushbroom HSI system represents a rapid and non-destructive method, suitable for applications in the industrial field for the quality control of final electronic products and the identification of defects and highly oxidised copper substrates. However, the challenge represented by irregular oxide film growth must be overcome to enable a better understanding of the impact of the oxide layer thickness on processes such as gluing and bonding and, hence, on the process control.

References

1. A. Ghosh and B. Corves, *Introduction to Micromechanisms and Microactuators*, Springer India, New Delhi, India (2015).
2. K. Hromadka, J. Stulik, J. Reboun and A. Hamacek, "DBC technology for low cost power electronic substrate manufacturing", *Procedia Eng.* **69,** 1180–1183 (2014). https://doi.org/10.1016/j.proeng.2014.03.107
3. J.M. Nowful, S.C. Lok and S.-W. Ricky Lee, "Effects of plasma cleaning on the reliability of wire bonding", in *Proc. Int. Symp. Electron. Mater. Packag., 3rd*, Jeju Island, South Korea, pp. 39–43 (2001). https://doi.org/10.1109/EMAP.2001.983955
4. Y. Long, F. Dencker, A. Isaak, J. Hermsdorf, M. Wurz and J. Twiefel, "Self-cleaning mechanisms in ultrasonic bonding of Al wire", *J. Mater. Process. Technol.* **258,** 58–66 (2018). https://doi.org/10.1016/j.jmatprotec.2018.03.016
5. G.D. Davis, "Contamination of surfaces: Origin, detection and effect on adhesion", *Surf. Interface Anal.* **20(5),** 368–372 (1993). https://doi.org/10.1002/sia.740200507
6. J.J. Kim and S.-K. Kim, "Optimized surface pretreatments for copper electroplating", *Appl. Surf. Sci.* **183(3–4),** 311–318 (2001). https://doi.org/10.1016/S0169-4332(01)00585-2
7. Y. S. Gong, C. Lee and C.K. Yang, "Atomic force microscopy and Raman spectroscopy studies on the oxidation of Cu thin films", *J. Appl. Phys.* **77(10),** 5422–5425 (1995). https://doi.org/10.1063/1.359234
8. C.T. Chong, A. Leslie, L.T. Beng and C. Lee, "Investigation on the effect of copper leadframe oxidation on package delamination", in *IEEE Electron. Compon. Technol. Conf., 45th*, Las Vegas, NV, USA, pp. 463–469 (1995). https://doi.org/10.1109/ECTC.1995.515322
9. S.K. Lahiri, N.K. Waalib Singh, K.W. Heng, L. Ang and L.C. Hog, "Kinetics of oxidation of copper alloy leadframes", *Microelectronics J.* **29(6),** 335–341 (1998). https://doi.org/10.1016/S0026-2692(97)00052-9
10. A. Shui, W. Zhu, L. Xu, D. Qin and Y. Wang, "Green sonochemical synthesis of cupric and cuprous oxides nanoparticles and their optical properties", *Ceram. Int.* **39(8),** 8715–8722 (2013). https://doi.org/10.1016/j.ceramint.2013.04.055
11. H.A. Macleod, *Thin Film Optical Filters*. CRC Press, Boca Raton, FL, USA (2010).
12. M. Langlet, K. Kartouni and D. Delahaye, "Characterization of copper oxidation by linear potential sweep voltammetry and UV-visible-NIR diffuse reflectance spectroscopy", *J. Appl. Electrochem.* **21(8),** 697–702 (1991). https://doi.org/10.1007/BF01034048
13. M.J. Graham, "Recent advances in oxide film characterization", *Pure Appl. Chem.* **64(11),** 1641–1645 (1992). https://doi.org/10.1351/pac199264111641
14. B. Balasubramanian, B.R. Mehta, D. Avasthi, F. Singh, A.K. Arora, M. Rajalakshmi, G. Raghavan, A. Tyagi and S.M. Shivaprasad, "Modifying the nanocrystalline characteristics—Structure, size, and surface states of copper oxide thin films by high-energy heavy-ion irradiation", *J. Appl. Phys.* **92(6),** 3304–3310 (2002). https://doi.org/10.1063/1.1499752

15. O. Messaoudi, H. Makhlouf, A. Souissi, I.B. Assaker, M. Karyaoui, A. Bardaoui, M. Oueslati and R. Chtourou, "Correlation between optical and structural properties of copper oxide electrodeposited on ITO glass", *J. Alloys Compd.* **611(25),** 142–148 (2014). https://doi.org/10.1016/j.jallcom.2014.05.055

16. P.J. Whiteside, J.A. Chininis and H.K. Hunt, "Techniques and challenges for characterizing metal thin films with applications in photonics", *Coatings* **6(3),** 35 (2016). https://doi.org/10.3390/coatings6030035

17. B. Lefez and M. Lenglet, "Photoluminescence of thin oxide layers on metallic substrates (Cu_2O/Cu and ZnO/Zn)", *Chem. Phys. Lett.* **179(3),** 223–226 (1991). https://doi.org/10.1016/0009-2614(91)87027-9

18. D. Gallant, M. Pezolet and S. Simard, "Optical and physical properties of cobalt oxide films electrogenerated in bicarbonate aqueous media", *J. Phys. Chem. B* **110(13),** 6871–6880 (2006). https://doi.org/10.1021/jp056689h

19. G.C. Allen and G.A. Swallow, "Reflectance spectroscopy of oxide films. II. Oxide layers on chromium metal", *Oxid. Met.* **17(1–2),** 157–176 (1982). https://doi.org/10.1007/BF00606198

20. S.R. de Sanchez, L.E. Berlouis and D.J. Schiffrin, "Difference reflectance spectroscopy of anodic films on copper and copper base alloys", *J. Electroanal. Chem. Interfacial Electrochem.* **307(1–2),** 73–86 (1991). https://doi.org/10.1016/0022-0728(91)85540-6

21. M. Dahrul and H. Alatas, "Preparation and optical properties study of CuO thin film as applied solar cell on LAPAN-IPB satellite", *Procedia Environ. Sci.* **33,** 661–667 (2016). https://doi.org/10.1016/j.proenv.2016.03.121

22. B. Lefez, K. Kartouni, M. Lenglet, D. Rönnow and C.G. Ribbing, "Application of reflectance spectrophotometry to the study of copper (I) oxides (Cu_2O and Cu_3O_2) on metallic substrate", *Surf. Interface Anal.* **22(1–12),** 451–455 (1994). https://doi.org/10.1002/sia.740220196

23. J.M. Machefert, A. D'Huysser, M. Lenglet, J. Lopitaux and D. Delahaye, "Initial stage of copper thermal oxidation studied by UV-vis-NIR reflectance spectroscopy, XPS and X-ray diffraction", *Mater. Res. Bull.* **23(10),** 1379–1388 (1988). https://doi.org/10.1016/0025-5408(88)90262-0

24. J. Stiedl, S. Green, T. Chassé and K. Rebner, "Characterization of oxide layers on technical copper material using ultraviolet visible (UV–Vis) spectroscopy as a rapid on-line analysis tool", *Appl. Spectrosc.* **73(1),** 59–66 (2018). https://doi.org/10.1177/0003702818797959

25. A.A. Gowen, C.P. O'Donnell, M. Taghizadeh, P.J. Cullen, J.M. Frias and G. Downey, "Hyperspectral imaging combined with principal component analysis for bruise damage detection on white mushrooms (*Agaricus bisporus*)", *J. Chemometr.* **22(3–4),** 259–267 (2008). https://doi.org/10.1002/cem.1127

26. Y. Peng and W. Wang, "Prediction of pork meat total viable bacteria count using hyperspectral imaging system and support vector machines", in *Food Processing Automation Conference Proceedings*, Providence, RI, USA (2008). https://doi.org/10.13031/2013.24558}

27. Z. Xiong, D.-W. Sun, Q. Dai, Z. Han, X.-A. Zeng and L. Wang, "Application of visible hyperspectral imaging for prediction of springiness of fresh chicken meat", *Food Anal. Methods* **8(2),** 380–391 (2015). https://doi.org/10.1007/s12161-014-9853-3

28. G. Polder, G. van der Heijden and I.T. Young, "Spectral image analysis for measuring ripeness of tomatoes", *Trans. ASAE* **45(4),** 1155–1161 (2002). https://doi.org/10.13031/2013.9924

29. B. Park, K.C. Lawrence, W.R. Windham and D.P. Smith, "Performance of hyperspectral imaging system for poultry surface fecal contaminant detection", *J. Food Eng.* **75(3),** 340–348 (2006). https://doi.org/10.1016/j.jfoodeng.2005.03.060

30. G. Lu and B. Fei, "Medical hyperspectral imaging: a review", *J. Biomed. Opt.* **19(1),** 010901 (2014). https://doi.org/10.1117/1.JBO.19.1.010901

31. F. Gruber and P. Wollmann (inventor), Fraunhofer Gesellschaft zur Forderung der Angewandten Forschung (assignee), *Anordnung zur Bestimmung der erreichbaren Haftfestigkeit vor Ausbildung einer stoffschlüssigen Verbindung an einer Oberfläche eines Fügepartners*. Deutschland Patent DE102015217091A1 (7/9/2015).

32. F. Gruber, P. Wollmann, B. Schumm, W. Gählert and S. Kaskel, "Quality control of slot-die coated aluminum oxide layers for battery applications using hyperspectral imaging", *J. Imaging* **2,** 12 (2016). https://doi.org/10.3390/jimaging2020012

33. S.H. Ham, M. Ferie, C. Carteret, G. Fricout, J. Angulo and F. Capon, "Hyperspectral imaging as an analytical tool for thin single and multilayer oxides characterization: A laboratory study", in *Workshop on Hyperspectral Image and Signal Processing: Evolution in Remote Sensing, 8th*, Los Angeles, CA, USA (2016). https://doi.org/10.1109/WHISPERS.2016.8071737

34. P. Wollmann, W. Gählert and E. Weißenborn (inventor), Fraunhofer Gesellschaft zur Forderung der Angewandten Forschung (assignee), *Arrangement for Spatially Resolved Determination of the Specific Electrical Resistance and/or the Specific Electrical Conductivity of Samples*. USA Patent US20180045758A1 (15/2/2018).

35. G. Bonifazi and S. Serranti, "Hyperspectral imaging based techniques in fluff characterization", *Proc. SPIE* **6377,** 63770O (2006). https://doi.org/10.1117/12.684661

36. H. Zhu, B. Chu, Y. Fan, X. Tao, W. Yin and Y. He, "Hyperspectral imaging for predicting the internal quality of kiwifruits based on variable selection algorithms and chemometric models", *Scientific Reports* **7,** 7845 (2017). https://doi.org/10.1038/s41598-017-08509-6

37. M. Zhao, C. Esquerre, G. Downey and C.P. O'Donnell, "Process analytical technologies for fat and moisture determination in ground beef - a comparison of guided microwave spectroscopy and near infrared hyperspectral imaging", *Food Control* **73(B),** 1082–1094 (2017). https://doi.org/10.1016/j.foodcont.2016.10.023

38. J. Sun, B. Ma, J. Dong, R. Zhu, R. Zhang and W. Jiang, "Detection of internal qualities of hami melons using hyperspectral imaging technology based on variable selection algorithms", *J. Food Process Eng.* **40,** 3 (2017). https://doi.org/10.1111/jfpe.12496

39. B. Karlsson, C.G. Ribbing, A. Roos, E. Valkonen and T. Karlsson, "Optical properties of some metal oxides in solar absorbers", *Phys. Scr.* **25(6A),** 826–831 (1982). https://doi.org/10.1088/0031-8949/25/6A/044

40. A. Baiano, C. Terracone, G. Peri and R. Romaniello, "Application of hyperspectral imaging for prediction of physico-chemical and sensory characteristics of table grapes", *Comput. Electron. Agr.* **87,** 142–151 (2012). https://doi.org/10.1016/j.compag.2012.06.002

41. G. Ahuja, S. Jaiswal and R.N. Chubbar, "Starch biosynthesis in relation to resistant starch" in *Resistant Starch - Sources, Applications and Health Benefits*, Ed by Y.-C. Shi and C. C. Maningat. John Wiley & Sons, UK, pp. 2–8 (2013).

42. S.-J. Cho, K.-W. Paik and Y.-G. Kim, "The effect of the oxidation of Cu-base leadframe on the interface adhesion between Cu metal and epoxy molding compound", in *IEEE Trans. Compon., Packag., Manuf. Technol., Part B.* **20(2),** 167–175 (1997). https://doi.org/10.1109/96.575569

43. B.H. Moon, H.Y. Yoo and K. Sawada, "Optimal oxidation control for enhancement of copper lead frame-EMC adhesion in packaging process", in *IEEE Electron. Compon. Technol. Conf.*, Seattle, WA, USA (1998). https://doi.org/10.1109/ECTC.1998.678861

44. G.R. Berriche, S.C. Vahey and B.A. Gillet, "Effect of oxidation on mold compound-copper leadframe adhesion", in *Proc. - Int. Symp. Adv. Packag. Mater.*, Braselton, GA, USA (1999). https://doi.org/10.1109/ISAPM.1999.757291

45. T.-G. Kang, I.-S. Park, J.-H. Kim and K.-S. Choi, "Characterization of oxidized copper leadframes and copperepoxy molding compound interface adhesion in plastic package", in *Proc. - Int. Conf. Adhes. Joining Coat. Technol. Electron. Manuf.*, Binghamton, NY, USA (2002). https://doi.org/10.1109/ADHES.1998.742011

46. R. Berriche, R. Lowry and M.I. Rosenfield, "An oxidation study of Cu leadframes", in *Proc. - Int. Symp. Adv. Packag. Mater.*, Braselton, GA, USA (1999). https://doi.org/10.1109/ISAPM.1999.757326